

Conduction-electron scattering from vacancies in copper

D. E. Simanek

Physics Department, Lock Haven University, Lock Haven, Pennsylvania 17745

A. J. Baratta* and A. Lodder

Natuurkundig Laboratorium, Vrije Universiteit, 1007 MC Amsterdam, The Netherlands

A. C. Ehrlich

U.S. Naval Research Laboratory, Washington, D.C. 20375

(Received 11 March 1987)

The first experimental results of the anisotropy of the conduction-electron scattering from vacancies in Cu are reported. The method used to study the electron-vacancy scattering rate is magnetic-field-induced surface-state resonance. The results show that the scattering rate in the $\{110\}$ plane of Cu varies by a factor of 2 over the Fermi surface. It is highest near the $\langle 100 \rangle$ axis and $\langle 111 \rangle$ neck and lowest at the $\langle 110 \rangle$ and $\langle 112 \rangle$ axes. A partial-wave analysis was performed and the Friedel phase shifts determined. This analysis shows the vacancy to have a predominantly *sp* character. The results for Cu are compared with de Haas-van Alphen data in Au and marked differences are noted. A companion paper analyzes the scattering rates in both Cu and Au with vacancies in terms of the cluster-defect formalism based on the Korringa-Kohn-Rostoker Green's-function method.

I. INTRODUCTION

Self-defects in metals result from a variety of causes including heating followed by rapid quenching, cold working, and radiation damage. The resulting defects include vacancies, Frenkel pairs, and more complex structures such as dislocations and voids. Probably the simplest such defect from both a structural and an electronic viewpoint is the vacancy. While a wealth of data is available on the scattering of conduction electrons from defects consisting of substitutional and interstitial atoms in dilute metal alloys,¹⁻⁴ a markedly smaller amount of information is available on such self-defects. The data that are available include de Haas-van Alphen (dHvA) studies of edge dislocations,⁵ dislocation loops in Cu,⁶ and vacancies in Au,^{7,8} as well as numerous resistivity studies.

For vacancies in Cu, no dHvA or similar scattering anisotropy measurements have been reported until now. In this paper, we report on the first investigation of anisotropic conduction-electron scattering by vacancies in Cu as measured by magnetic-field-induced surface-state resonances. These measurements show a marked anisotropy with the scattering rate highest near the $\langle 100 \rangle$ axis and the $\langle 111 \rangle$ neck. Comparison of the results obtained here with those obtained for vacancies in Au reveals significantly different behavior for these two noble metals. In companion paper, we report on theoretical calculations performed to explain the differences and to understand better the electronic structure of the defect.

In the next two sections, the magnetic-field-induced surface-state technique will be briefly reviewed along with a description of the experiment. In the final section, the electron-vacancy scattering rates for Cu will be presented and their implications discussed.

II. MAGNETIC-FIELD-INDUCED SURFACE-STATE METHOD

In this section, only the basic methodology of the magnetic-field-induced surface-state method will be reviewed. For a more detailed discussion, the work of Prange and Nee^{9,10} and Doezema and Koch¹¹ should be consulted. Here it will be sufficient to describe briefly how this method may be used to obtain electron-scattering rates.

In the presence of a weak magnetic field, Prange and Nee⁹ have shown that electrons in the near-surface region can become trapped in a triangular potential well. The results are quantized energy states with a characteristic lifetime τ (see Fig. 1). Transitions may be induced between such states using microwave or infrared radiation provided the magnetic field is equal to the resonant field H_{mn} given by

$$H_{mn} = \frac{\hbar}{e} \left[\frac{\omega}{a_n - a_m} \right]^{3/2} \left[\frac{2K}{v_F^3} \right]^{1/2}; \quad (1)$$

ω is the microwave frequency, a_m and a_n are the m th and n th zero of the Airy function, K the local radius of curvature of the Fermi surface, and v_F the Fermi velocity. Only those regions of the Fermi surface for which K/v_F^3 has an extreme value will contribute. Such regions are typically $3-10^\circ$ in length and $1-2^\circ$ in width with respect to the center of the Brillouin zone.

At microwave frequencies, the resonances may be observed using a conventional reflection-type spectrometer similar to those used in cyclotron resonance studies.¹¹ In such a system, the sample forms one wall of a cylin-

drical cavity. As a resonance is approached, the energy absorption increases due to a change in the surface impedance of the sample resulting from transitions between surface states. This in turn produces a change in the Q of the cavity which is measurable using a synchronous

detection system.

In the actual experiment, the derivative of the real part of the surface impedance Z with respect to H is measured. The shape of the resonance spectrum is given by

$$\operatorname{Re} \left[\frac{dZ}{dH} \right] = \operatorname{Re} [\operatorname{const} \times (i - \sqrt{3})] \frac{d}{dH} \int dk_y \left[\frac{v_x^2(k_y)}{v_F(k_y)} \sum_{m,n} \frac{\alpha_{mn}^2(k_y, H, \delta)}{\omega - \omega_{mn}(H, k_y) + i\Gamma(k_y, H)} \right], \quad (2)$$

where k_y is the k -space coordinate along the magnetic field. The quantity α_{mn} is a matrix element between the surface-state wave functions ϕ_m and ϕ_n and the electric field in the anomalous-skin-effect skin depth δ of the metal. The quantity v_x is the component of the Fermi velocity along the rf electric field. The quantity ω_{mn} is the energy difference between the m th and the n th surface state divided by \hbar . The term $i\Gamma$ is a dispersive term accounting for electron scattering. The quantity Γ is the scattering rate.

When there are several distinguishable and noninteracting scattering mechanisms then the scattering rate Γ is the sum of the individual rates. In the relaxation-time approximation, this implies of course that the scattering rate is the sum of inverse relaxation times. Prange and Nee⁹ suggested that for surface states three processes contribute to the scattering rate, bulk-defect scattering, surface scattering, and phonon scattering. Γ can then be written as a sum of three terms. If one uses the relaxation-time approximation for the bulk term then

$$\Gamma = \frac{1}{\tau_{\text{defect}}} + \Gamma_{\text{surface}} + \Gamma_{\text{phonon}}. \quad (3)$$

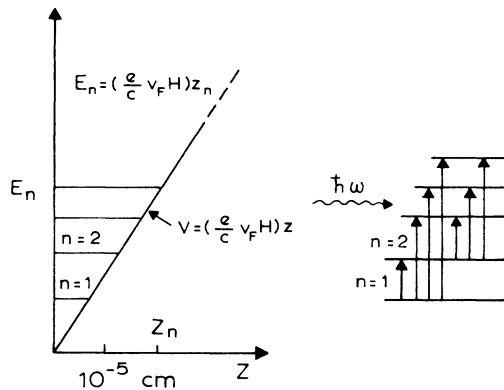


FIG. 1. Triangular potential well formed by magnetic potential V due to magnetic field H and the crystal surface potential. The quantity z is the depth into the sample and v_F the Fermi velocity. Shown are the first few energy levels, quantized penetration depth z_n , and corresponding energy of the state E_n .

By measurement of the surface-state resonance spectrum in the pristine metal and in the damaged metal, one may obtain the change in scattering rate attributable to the damage. This approach is that which was used by the authors. As discussed elsewhere,^{3,12} the values of $1/\tau$ obtained from the experiment are local values compared to orbital averages obtained from dHvA Dingle temperature measurements. Such local values can of course be combined to obtain the Dingle temperatures for various dHvA orbits. This allows for direct comparison with dHvA data.

III. EXPERIMENT

A. Apparatus

The apparatus consists of a reflection-type microwave spectrometer operating at 24 GHz, a set of Helmholtz coils, sample holder, and a synchronous detection system. The coils can be manually rotated through 360° with respect to the sample holder. The sample holder located at the end of one arm of the microwave spectrometer contains the copper sample which forms one wall of a cylindrical microwave cavity. The sample and holder are immersed in a bath of liquid helium (nominally 4.2 K).

The magnetic field strength H is modulated at 25 Hz and is slowly swept from 0 to 20 Oe over a time interval of 10–15 min. A microwave diode detector demodulates this signal from the 24 GHz microwave “carrier” frequency. The signal is then amplified and processed with a lock-in amplifier. The resulting signal is a direct measurement of the cavity Q , and is proportional to dR/dH . The plot of dR/dH versus H represents a surface-state “spectrum.”

B. Samples

The copper sample was spark cut from a 99.999% pure single-crystal boule. It was oriented along the $\{110\}$ crystal plane and annealed in a partial (4×10^{-4} mm Hg) oxygen atmosphere at 1000°C for 10 days. The sample surface was then hand lapped with 600 grit emery paper and distilled water and then electropolished for 4 h in a 2:1 solution of phosphoric acid to water, following the method of Tegart.¹³

Prior to heating and quenching, scattering rate mea-

measurements were made on this sample in the manner described in the next section. The sample was then subjected to a heating and quenching operation to achieve a fixed concentration of vacancies in it. For the heating, the copper sample was surrounded by purified argon while it was held at a constant temperature above 600°C for 30 min. It was then quenched by quickly lowering it into a liquid nitrogen and isopentane bath (temperature about -160°C).

The equilibrium concentration of vacancies was estimated using the expression¹⁴

$$C_{\text{vac}} = K_0 \exp(-E_s / k_B T),$$

where C_{vac} is the vacancy concentration in ppm at temperature T , K_0 is 4.32×10^6 ppm, k_B Boltzmann's constant, and T the temperature in degrees Kelvin. E_s is the free enthalpy for vacancies in solution in copper. A value of 1.17 ± 0.11 was used for E_s .¹⁴

The temperature of the sample was monitored with an ir photometer during heating. However, due to uncertainties in the ir emissivity of the sample, (0.4–0.8) the temperature value is uncertain, being between 600 and 725°C. This corresponds to a range of vacancy concentrations between 0.8 and 5.5 ppm. Because of the low vacancy concentration, sample geometry, and the nature of the surface-state effect, no attempts were made to measure the vacancy concentration directly (e.g., by resistivity).

In this regard it should be noted that the surface-state effect samples a region about 0.1 μm in depth and that we know of no straightforward analytical technique to accurately characterize that region, particularly since such a region would be expected to have a vacancy-concentration gradient associated with the quench-rate gradient. Furthermore, it was also not necessary to know the vacancy concentration accurately in this experiment since in the dilute limit the scattering-rate anisotropy is independent of concentration.

C. Scattering-rate measurements and analysis

Scattering rates were measured for nine localized regions on the Fermi surface in the {110} plane of copper, both before and after the heating and quenching operation (see Fig. 2). The method of analysis will be only briefly summarized here. A more complete description of the details of the fitting can be found in Doezema¹⁵ and Baratta and Ehrlich.³

Most of the dR/dH spectra will show not only several resonance peaks of a given spectral series, but also overlapping resonances from extrema at different locations on the Fermi surface. Because of this, many spectra cannot be reliably analyzed by the present curve-fitting methods. Also, some regions of the Fermi surface produce no resonances, so scattering-rate data cannot be obtained there. The region between $\varphi = 70^\circ$ and 90° is one such case.

Scattering rates as a function of Fermi surface location are determined by producing from Eq. (2) a computer-generated spectrum which best fits the experimentally obtained spectrum. The scattering rate is treat-

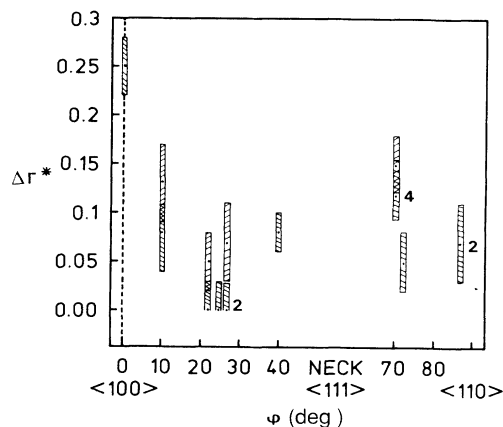


FIG. 2. Change in scattering rate Γ^* in {110} plane of Cu due to vacancies. the angle φ locates the region on the Fermi surface giving rise to the resonances. The angle φ is taken with respect to the $\langle 100 \rangle$ axis and the center of the zone. Numbers besides certain data points give the number of independent fits yielding the same value of Γ^* . The uncertainty in each measurement is shown by the crosshatched areas. These are taken at one standard deviation.

ed as an adjustable parameter with the other parameters varying in a predictable way over the Fermi surface.

This fitting process itself is the dominant error source, the effect of all other experimental variables being negligible. An estimate of the uncertainty introduced by the fitting may be obtained by noting that computer-generated spectra were only available for $1/\Gamma^* = 1, 1.5, 2, 2.5, \dots$, where Γ^* equals the scattering rate Γ divided by ω the microwave frequency. The increment in $1/\Gamma^*$ is then 0.5. This increment was just large enough to show a difference in quality of fit when the computer generated spectra were fitted to the experimentally obtained spectrum. Thus for any given fit, the range in uncertainty of $1/\Gamma^*$ is ± 0.25 , or less than 10% in most cases. To determine the uncertainty in $\Delta\Gamma^*$, these uncertainties were combined by summing in quadrature, assuming independence of fits. The result is treated as a 68% confidence interval (or one standard deviation). This gives standard deviations of about 5–12% in the scattering rates observed in this experiment (second or third column, Table I), and 15–43% in the change in scattering rates; (fourth column, Table I).

D. Experimental results

Table I shows all relevant data on all those experimental resonance curves for which reasonably good fits were obtained. The first column gives φ , the angle locating the region of the Fermi surface from which the signal originates. It is measured with respect to the $\langle 100 \rangle$ axis. The second column gives the experimentally fitted scattering rate Γ^* of the "pure" copper. The third column gives the experimentally fitted scattering rate Γ^* of the copper with vacancies. The fourth column gives the change in scattering rate $\Delta\Gamma^*$. Figure 2 is a plot of the $\Delta\Gamma^*$ data as a function of Fermi-surface location φ .

TABLE I. Summary of scattering rate results. Scattering rates Γ^* in the $\{110\}$ plane of pure copper, and copper with vacancies, versus the angle φ . The angle φ is measured from the $\langle 100 \rangle$ axis, and locates the resonant electrons on the Fermi surface. Uncertainties are standard deviations.

φ (deg)	Scattering rate Γ^*		Change in scattering rate $\Delta\Gamma^*$
	Pure copper	Copper with vacancies	
90	0.33±0.02	0.40±0.03	0.07±0.04
70	0.25±0.01	0.40±0.03	0.15±0.03
27	0.33±0.02	0.33±0.02	0.00±0.03
27	0.33±0.02	0.40±0.03	0.07±0.04
90	0.33±0.02	0.40±0.03	0.07±0.04
70	0.28±0.02	0.40±0.03	0.12±0.04
10	0.20±0.03	0.33±0.02	0.13±0.04
10	0.20±0.03	0.28±0.02	0.08±0.04
70	0.28±0.02	0.40±0.03	0.12±0.04
70	0.28±0.02	0.40±0.03	0.12±0.04
25	0.33±0.02	0.33±0.02	0.00±0.03
27	0.33±0.02	0.33±0.02	0.00±0.03
70	0.28±0.02	0.40±0.03	0.12±0.04
72	0.28±0.02	0.33±0.02	0.05±0.03
22	0.28±0.02	0.33±0.02	0.05±0.03
22	0.28±0.02	0.28±0.02	0.00±0.03
40	0.25±0.01	0.33±0.02	0.08±0.02
0	0.25±0.01	0.50±0.03	0.25±0.03

The scattering-rate results in Fig. 2 clearly show that the vacancy-induced scattering is anisotropic over the Fermi surface. The scattering rate is highest in the $\langle 100 \rangle$ direction and near the neck. It is lowest around $\varphi=20^\circ-30^\circ$ from the $\langle 100 \rangle$ axis (a “belly” region) and at the $\langle 110 \rangle$ axis. The ratio of neck to belly scattering rates is approximately 2.

IV. DISCUSSION

While no comparable work for Cu has been reported, it is possible to compare the data reported here with low-field Hall-effect measurements. Lengeler and Papastaikoudis¹⁶ have measured the low-field Hall coefficient in quenched Cu with approximately 30 ppm of vacancies. They found the coefficient for Cu to be $-6.2 \times 10^{-5} \text{ cm}^3/\text{C}$.

The scattering rates measured here can be related to

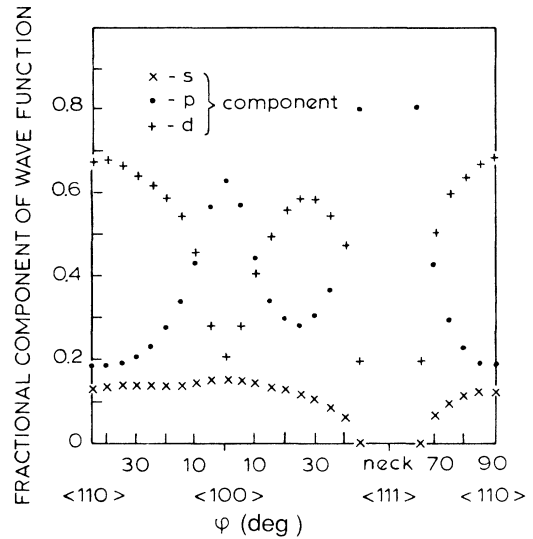


FIG. 3. Fraction of s , p , and d states in Cu electron wave function due to Coleridge (Ref. 18). The angle is measured with respect to the center of the zone and the $\langle 100 \rangle$ axis.

the Hall coefficient using a three-band model and the average of the scattering rates over the corresponding Fermi-surface regions.¹⁷ To calculate the Hall coefficient from the data reported here, the Fermi surface was divided into the three regions identified in Table II. These regions correspond to those suggested by Dugdale and Furth¹⁷ and were used successfully by the authors in a previous paper.³ The average scattering rate for each region was determined and the Hall coefficient calculated. This yields a value of $-5.2 \times 10^{-5} \text{ cm}^3/\text{C}$ for the reduced Hall coefficient with an uncertainty of $\pm 25\%$. This result is in very good agreement with the measured values reported by Lengeler and Papastaikoudis.

A widely used method for describing scattering by a localized potential is the partial wave method, which is applicable to those situations where only s -, p -, and d -wave scattering are important. The method treats the scattering anisotropy as due to the variations of hybridization of the electronic wave functions over the Fermi surface and to a “weighting” or “scattering parameter” for each partial wave component.¹⁸

TABLE II. Friedel phase shifts. Fitted Friedel phase shifts obtained by fitting Eq. (4) to data in Table I. The neck-to-belly and $\langle 110 \rangle$ -axis-to-belly scattering ratios compare the average scatter rates in these regions of the Fermi surface, in the $\{110\}$ plane. For the $\langle 110 \rangle$ axis, $\varphi=0^\circ-15^\circ$; the belly, $\varphi=15^\circ-35^\circ$; neck, $\varphi=45^\circ$.

	Value	Standard deviation
s -wave phase shift (rad)	0.75	0.5
p -wave phase shift (rad)	0.72	0.1
d -wave phase shift (rad)		negligible
Neck-to-belly scattering ratio	1.7	0.5
$\langle 110 \rangle$ -axis-to-belly scattering ratio	2.2	0.5

TABLE III. Dingle temperatures for Au and Cu vacancy systems. Comparison of experimentally measured Dingle temperatures for Au (Ref. 8) with those for Cu calculated from measured scattering rates and Eqs. (4) and (5). $B\langle 100 \rangle$ denotes the belly $\langle 100 \rangle$ de Haas-van Alphen orbit and $N\langle 111 \rangle$ denotes the neck $\langle 111 \rangle$ de Haas-van Alphen orbit, etc.

	Au(vacancy) T_d^* (K/at. %)	Cu(vacancy) T_d^* (K/at. %)
$B\langle 100 \rangle$	38.2 ± 2.5	18.9
$B\langle 111 \rangle$	38.7 ± 1.1	17.5
$N\langle 111 \rangle$	33.8 ± 2.4	27.5
$N\langle 111 \rangle$	0.88	1.46
$B\langle 100 \rangle$		
$N\langle 111 \rangle$	0.87	1.57
$B\langle 111 \rangle$		

Figure 3 shows the variation of fractional contributions of the s , p , and d components of the copper electron wave function at the Fermi energy in the $\{110\}$ plane.¹⁹ If Fig. 3 is compared with the experimental data of Fig. 2, a preliminary conclusion can be immediately drawn. The experimentally observed anisotropy shows high scattering near the neck of the Fermi surface and near the $\langle 100 \rangle$ axis, but low scattering in the region around $\varphi = 25^\circ$. This resembles the variation of p -wave contribution over the Fermi surface, except that the observed scattering is substantially greater at the $\langle 100 \rangle$ axis than near the Fermi-surface neck. However, if s -wave scattering is also present it could account for the additional scattering observed near the $\langle 100 \rangle$ axis.

The small change in scattering rate near $\varphi = 25^\circ$ suggests that the vacancies scatter very little of the d -wave component. From Fig. 2 it is evident that the host wave function does have a substantial d -type character there. Therefore, the observed anisotropy would seem to be due predominantly to s - and p -type scattering by the vacancies, with very little d -type scattering.

A satisfactory fit was in fact obtained with about equal contributions of s - and p -wave components. The ratio of s - and p -wave contributions produced by the multiple-regression curve-fitting program was not significantly sensitive to the assumed amount of d -wave contribution, and therefore the d -wave contribution was taken to be negligible. Based on these results, these data suggest that the vacancy potential possesses predominantly s and p character.

Using this approach, one may obtain a set of Friedel phase shifts by fitting the expression²⁰

$$\frac{\Gamma}{v_F} = \frac{1}{v_F \tau} = \frac{16\pi c}{k_F^2 a^3} \sum_{l=0}^2 \frac{C_k t_k^l}{v_F} \sin^2 \varphi_l \quad (4)$$

to the measured data. Here a is the lattice constant, c the concentration of scatterers in atomic fraction, t_k^l the amplitude of the host wave function, φ_l the Friedel phase shift and $C_k = k^2/2\pi\hbar$. The resulting phase shifts are given in Table II. For these calculations, a vacancy

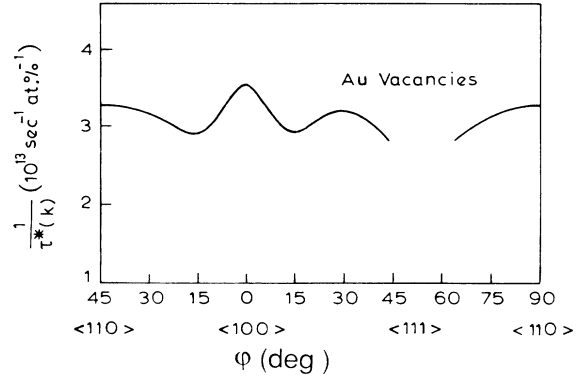


FIG. 4. Anisotropy of the conduction electron scattering rate from vacancies in Au as determined by Lengeler (Ref. 8) using dHvA Dingle temperatures and Eq. (5).

concentration of 2 ppm was assumed. Again it is evident that the vacancy potential is in fact predominantly an sp scatterer since the Friedel phase shift is essentially zero for the d -wave component. This analysis assumes that lattice distortion which is definitely present does not significantly contribute to the scattering. As will be seen in the accompanying paper, this is in fact true for Cu.

In an attempt to better understand the origin of the observed anisotropy, the results for Cu were compared to results reported by Lengeler⁸ for vacancy-induced scattering in Au. Using the de Haas-van Alphen technique, Dingle temperatures were measured for ten dHvA orbits. The results are summarized in Table III. Local values of $1/\tau^*$ were also calculated by Lengeler through inversion of the expression for the Dingle temperatures T_D^*

$$T_D^* m_c^* = \frac{\hbar^2}{(2\pi)^2 k_B} \int \frac{k_{\perp}^2}{\mathbf{v}^* \cdot \mathbf{k}_{\perp}} \frac{1}{\tau^*(k)} d\eta, \quad (5)$$

where $\tau^*(k)$ is the local scattering rate and η the angle locating the k point on the cyclotron orbit. The weight factor $k^2/(\mathbf{v}^* \cdot \mathbf{k}_{\perp})$ depends on the Fermi surface geometry and velocities. Figure 4 is a plot of the resulting scattering rates. This should be compared with the anisotropy for vacancies in Cu given in Fig. 2. Finally, Dingle temperatures for the Cu vacancy system were calculated from the results reported here. These are also given in Table III.

A comparison of the Dingle temperatures in Au and Cu and their ratios reveals that the neck-to-belly ratios are greater than 1 for Cu and less than 1 for Au. Furthermore, there is little anisotropy of the scattering rate for Au compared to Cu. The problem then is to account for the differences in the observed anisotropy for these two noble metals.

A simple model of the vacancy cannot explain these results as Lengeler has already shown. He found that a model in which the vacancy is represented by a constant potential within the muffin-tin sphere associated with the

scattering center produced neck Dingle temperatures for Au that were too small compared to the belly Dingle temperatures. Upon reflection, Lengeler suggested that the failure of this simple model to account for lattice distortion might be the cause of the disagreement.

Recently a Korringa-Kohn-Rostoker Green's function method has been formulated²¹ and elaborated numerically²² for the very purpose of analyzing situations in which lattice distortion and charge transfer contribute. Using this method, in a companion paper²³ Lengeler's hypothesis is explored for both Cu and Au as well as the ability of self-consistent potentials to represent the measured anisotropy in Cu.

ACKNOWLEDGMENTS

The authors wish to express their gratitude to the staff of the Metal Physics Branch, in particular Dr. G. Kamm, of the U.S. Naval Research Laboratory (NRL), Washington, D.C. for their assistance in this work. We also wish to acknowledge the joint sponsorship of the American Society of Engineering Educators and the Office of Naval Research for supporting a portion of this work. Finally we wish to acknowledge the valuable assistance of Dr. R. Meussner (NRL) and Tom Gillen and Dr. D. Frankel (both from Pennsylvania State University).

*Permanent address: The Pennsylvania State University, University Park, PA 16802.

¹R. G. Poulson, D. L. Randles, and M. Springford, *J. Phys. F* **4**, 981 (1974).

²P. T. Coleridge, I. M. Templeton, and P. Vasek, *J. Phys. F* **14**, 2963 (1984).

³A. J. Baratta and A. C. Ehrlich, *Phys. Rev. B* **28**, 4136 (1983).

⁴W. R. Wampler and B. Lengeler, *Phys. Rev. B* **15**, 4614 (1977).

⁵Y. K. Chang and R. J. Higgins, *Phys. Rev. B* **12**, 4261 (1975).

⁶Y. K. Chang, A. J. Arko, G. W. Crabtree, J. B. Ketterson, L. R. Windmiller, R. J. Higgins, and F. W. Young Jr., in *Fundamental Aspects of Radiation Damage in Metals*, edited by M. T. Robinson and F. W. Young, Jr. (National Technical Information Center, Springfield, VA, 1976), p. 846.

⁷Y. K. Chang and G. W. Crabtree, *Phys. Rev. B* **16**, 714 (1977).

⁸B. Lengeler, *Phys. Rev. B* **15**, 5504 (1977).

⁹R. E. Prange and T. W. Nee, *Phys. Rev.* **168**, 779 (1968).

¹⁰T. W. Nee, J. F. Koch, and R. E. Prange, *Phys. Rev.* **174**,

758 (1968).

¹¹R. E. Doezema and J. F. Koch, *Phys. Rev. B* **6**, 2071 (1972).

¹²A. J. Baratta and A. C. Ehrlich, *Phys. Rev. B* **24**, 517 (1981).

¹³W. J. Tegar, *The Electrolytic and Chemical Polishing of Metals in Research and Industry* (Pergamon, London, 1959).

¹⁴R. O. Simmons and R. W. Balluffi, *Phys. Rev.* **129**, 1533 (1963).

¹⁵R. E. Doezema, Ph.D. Thesis, Department of Physics and Astronomy, University of Maryland, 1971.

¹⁶B. Lengeler and C. Papastaikoudis, *Phys. Rev. B* **21**, 4368 (1980).

¹⁷J. S. Dugdale and L. D. Firth, *J. Phys. C* **2**, 1272 (1969).

¹⁸P. T. Coleridge, *J. Phys. F* **2**, 1016 (1972).

¹⁹P. T. Coleridge (private communication).

²⁰P. T. Coleridge, N. A. W. Holzwarth, and M. J. G. Lee, *Phys. Rev. B* **10**, 1213 (1974).

²¹A. Lodder, *J. Phys. F* **6**, 1885 (1976).

²²J. Molenaar and A. Lodder, *J. Phys. F* **13**, 1501 (1983).

²³A. J. Baratta, A. Lodder, and D. E. Simanek, following paper, *Phys. Rev. B* **36**, 9088 (1987).